Design of a High-Efficiency Wireless Power Transfer System With Intermediate Coils for the On-Board Chargers of Electric Vehicles

Duc Hung Tran, Van Binh Vu, and Woojin Choi, *Member, IEEE*

***Abstract*—In this paper, a high efficiency inductive wireless power transfer system for the on-board chargers of electric vehicles is proposed. In order to improve the power transfer efficiency, the proposed system adopts two additional intermediate coils with resonant capacitors, which increases the effective magnetizing impedance between the transmitter and receiver coils with no ferrites. The resonant tank of the proposed system is designed to operate the converter as a current source and as a voltage source at two different frequencies to implement the constant current (CC) mode charge and constant voltage (CV) charge, respectively. Since the proposed converter operates at a fixed frequency in each mode of charge operation, full soft switching of all the switching devices is possible and the zero phase angle condition can be achieved in both the CC and CV mode operations. A theoretical analysis based on a Thevenin model to come up with a suitable design for the battery charger and its closed-loop controller is presented and its superior performance is demonstrated by experimental results. A 6.6 kW prototype is implemented with a 200 mm air gap to demonstrate the validity of the proposed method. Experimental results show that the dc to dc conversion efficiency of the proposed system is 97.08% at 3.7 kW of output power in the CV mode charge.**

***Index Terms*—Constant current (CC)/constant voltage (CV) charge, electric vehicles (EVs), wireless power transfer (WPT), zero phase angle (ZPA).**

I. Introduction

UP TILL now, the most common method for charging electric vehicle (EV) batteries is plug-in charge, which connects an EV to the grid to charge its battery via a cable. However, this has some disadvantages such as being bulky and messy. In addition, exposure to electric plugs may cause safety issues for users. Wireless power transfer (WPT) topologies have got more attention during the last few years since they are able to transfer electrical energy without wire connections and allow devices to recharge more safely and conveniently, thereby eliminating most of the issues associated with their conventional wired counterparts [1]–[4].

In recent years, many studies on wireless chargers have been carried out and a well-known approach is the inductive WPT system employing two coil resonators for a short distance [5]–[10]. With this topology, it is possible to obtain a high efficiency in power transfer when the air gap is smaller than several centimeters. However, if the distance between the transmitter and the receiver is extended, the efficiency declines rapidly because of weak magnetic coupling. In order to enhance magnetic coupling, some researchers have proposed methods that use high permeability material such as ferrites. However, this contributes to increases in volume, weight which makes it unsuitable for EV applications [11]–[13]. It is also possible to achieve high efficiency at larger air-gaps in between 20 and 100 cm by operating the WPT converter at very high frequencies (MHz) thanks to the high quality factor of the coils. However, it is only suitable for low power applications (several tens of watts) since the transferred power is inversely proportional to the frequency. Hence, it cannot be applied for EV charger application of which power rating is several kW [14], [15].

Other approaches adopted intermediate coils to improve the effectiveness in coupling and three-coil systems have been proposed in [16]–[18]. In [18], a three-coil method is proposed to improve the efficiency of WPT systems with an intermediate coil and this study suggests the optimal position to place the intermediate coil in three coil WPT systems. In [17], a three coil system is further analyzed in detail to suggest a suitable design procedure for high-efficiency WPT systems and it is verified by experiments. However, this system cannot achieve full soft switching since it is not designed to achieve the zero phase angle (ZPA) condition during the entire charge operation. In addition, its soft switching range is narrow and a certain amount of switching loss is unavoidable. In particular, the loss in the primary switches is one of the major factors which impairs system efficiency. In order to further improve the coupling factor WPT topologies with two intermediate coils are presented in [19]–[21]. In [19], a WPT system adopting an asymmetric four-coil resonator is proposed. Since the intermediate coils help to boost the apparent coupling coefficient at the operating frequency, high power conversion efficiency can be achieved. However, it is not presented clearly as to how to maximize the apparent coupling coefficient in this paper. Moreover, since the converter is

Manuscript received August 30, 2016; revised October 31, 2016 and December 23, 2016; accepted January 22, 2017. Date of publication February 1, 2017; date of current version October 6, 2017. Recommended for publication by Associate Editor J. Acero.

D. H. Tran and V. B. Vu are with Electrical Engineering, Soongsil University, Seoul 156-743, South Korea (e-mail: duchungdktd@gmail.com; binh0591@gmail.com).

W. Choi is with Electrical Engineering, Soongsil University, Seoul 156-743, South Korea (e-mail: cwj777@ssu.ac.kr).

Color versions of one or more of the figures in this paper are available online at http://ieeexplore.ieee.org.

Digital Object Identifier 10.1109/TPEL.2017.2662067

See http://www.ieee.org/publications_standards/publications/rights/index.html for more information.

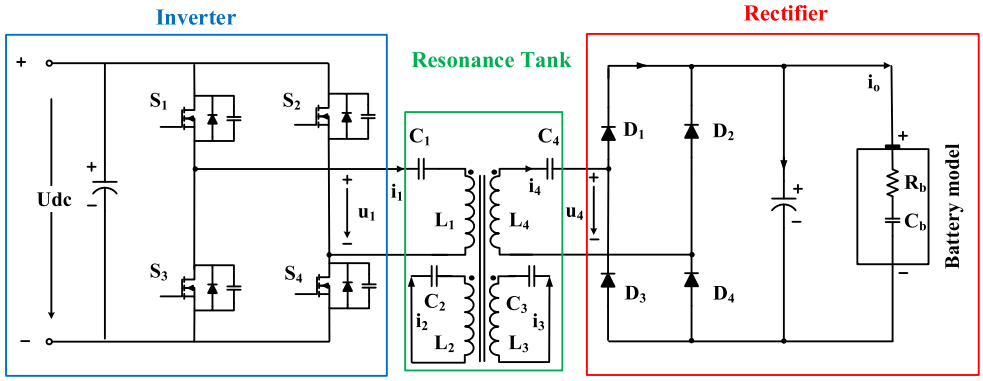

Fig. 1. Configuration of the proposed series–series compensated four-coil WPT system.

designed to operate at one frequency only for CV mode charge, it can hardly be applied for EV charger applications which require CC mode charge as well. In [21], some optimization technique for the compensation capacitor of the resonant tank is proposed to improve the efficiency of the WPT and it is applied to a 3.3 kW WPT charger. However, it has many disadvantages such as high turn-OFF current of the switches and heavy weight due to a lot of ferrite bars to achieve high coupling coefficient. The maximum efficiency obtained with the proposed method is only 92% at a 210 mm airgap, which is lower than that of its wired counterparts.

In addition to efficiency, it is also important to regulate the output to implement the constant current (CC) charge and constant voltage (CV) charge in charger applications. Since the most efficient and popular method for the charging of EV batteries is the CC/CV mode charge, it should be possible to implement it with WPT systems. However, this can be difficult to achieve without a wide range of frequency variation in case of resonant converters. In order to deal with this issue, a number of design and control guidelines have been presented in several recent publications [22]–[24]. In [22], a pulse frequency modulation (PFM) technique is used to control the output voltage of a converter to implement the CV mode charge. Hence, a wide range of frequency variation is inevitable and it is impossible to maintain the ZPA condition over the entire charge operation. Another approach is a combination of the phase shift and the PFM controls [23]. In this scheme, the soft switching of the primary switches can be achieved by using hardware to detect the zero crossing of the primary current. However, it is complex and expensive since it employs an additional dc–dc converter to regulate the output voltage.

In this paper, a novel WPT system using two intermediate coils with capacitors is proposed for the on-board charger of EV applications in order to overcome the above-mentioned drawbacks of the conventional WPT systems. The configuration of this system is shown in Fig. 1. With the help of two intermediate coils, the effective magnetizing impedance between the transmitter and the receiver coils is significantly increased to achieve a high-efficiency power transfer. The resonant tank of the converter is designed to operate the converter as a current source for the CC mode charge and as a voltage source for the CV mode charge. Since the proposed converter works at a fixed resonant frequency in each charge mode, the ZPA condition and full soft switching of all the switching devices can be achieved during the entire charge process. A mathematical model of the proposed system is presented and analyzed to show the principle of the proposed method. The detail design procedure to achieve the ZPA condition is also discussed.

TABLE I
SPECIFICATION OF THE WPT SYSTEM

Parameters	Symbol	Value
Nominal input voltage	$U_{\rm dc}$	400 V
Battery voltage	U_o	250–420 V
Rated output power	P_o	6.6 kW
Nominal charging current	I_o	15.7 A
Cut-off current	$I_{\rm co}$	1.57 A
Equivalent load impedance	R_o	17–267 Ω

This paper comprises five sections. In Section II, a general analysis of a series–series compensated four coil WPT system by Thevenin theorem is presented based on the fundamental harmonic approximation (FHA) method. The design procedure for the resonant tank and closed-loop PFM controller for each mode of charge is presented in Sections III and IV. Experimental results obtained with a 6.6 kW WPT converter with an air gap of 200 mm are presented in Section V to validate the design process. Finally, some conclusions are given in Section VI.

II. CIRCUIT CONFIGURATION AND OPERATION PRINCIPLE

A. First Harmonic Approximation Model of the Proposed Converter

Fig. 1 shows the proposed four-coil system. The circuit consists of a full-bridge inverter composed of four power MOSFET switches ($S_1 - S_4$), a loosely coupled transformer with two intermediate resonators, and a full–bridge diode rectifier. The specifications of the WPT system are shown in Table I, and the CC/CV charge profile of the EV battery and its equivalent impedance during charging is shown in Fig. 2.

In order to analyze the basic characteristics of the series–series four-coil compensation topology, the FHA method is used. By ignoring all of the high-order harmonics, the first harmonic approximated model of the circuit is then obtained as

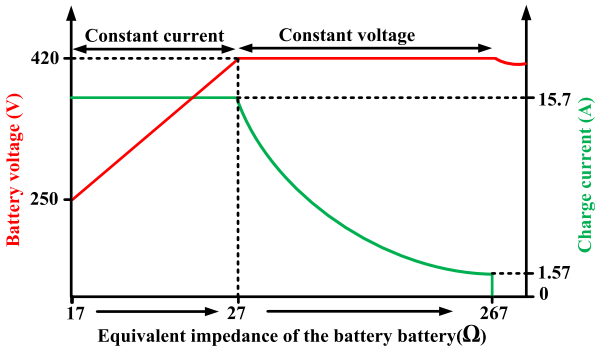

Fig. 2. CC/CV charge profile of the EV battery and its equivalent impedance of the battery during the charge.

shown in Fig. 2. The basic formula obtained with first harmonic approximation can be represented as

$$\begin{aligned} u_1(t) &= \frac{4}{\pi} U_{\mathrm{dc}} \cdot \sin(\omega \cdot t + \theta + \varphi) \\ i_1(t) &= I_1 \cdot \sin(\omega \cdot t + \theta) \\ u_4(t) &= \frac{4}{\pi} U_o \cdot \sin(\omega \cdot t) \\ i_4(t) &= I_4 \cdot \sin(\omega \cdot t) \\ I_4 &= \frac{\pi}{2} I_o \\ R_{L,\mathrm{eq}} &= \frac{8}{\pi^2} \frac{U_o^2}{P_o} \end{aligned} \tag{1}$$

where $u_1(t)$ is the fundamental harmonic voltage of the square wave input voltage of the tank, U_{dc} is the input voltage, and $R_{L,\mathrm{eq}}$ is the equivalent load resistance considering the battery charge profile during the CC/CV mode charge.

By applying Kirchhoff's voltage law to the circuit, the following voltage equations can be obtained

$$\begin{aligned} \frac{\hat{U}_1}{j\omega L_1} &= \left(1 - \frac{\omega_1^2}{\omega^2}\right)\hat{I}_1 + k_{12}\sqrt{\frac{L_2}{L_1}}\hat{I}_2 + k_{13}\sqrt{\frac{L_3}{L_1}}\hat{I}_3 \\ &\quad + k_{14}\sqrt{\frac{L_4}{L_1}}\hat{I}_4 \\ 0 &= k_{12}\sqrt{\frac{L_1}{L_2}}\hat{I}_1 + \left(1 - \frac{\omega_1^2}{\omega^2} n_{f21}^2\right)\hat{I}_2 + k_{23}\sqrt{\frac{L_3}{L_2}}\hat{I}_3 \\ &\quad + k_{24}\sqrt{\frac{L_4}{L_2}}\hat{I}_4 \\ 0 &= k_{13}\sqrt{\frac{L_1}{L_3}}\hat{I}_1 + k_{23}\sqrt{\frac{L_2}{L_3}}\hat{I}_2 + \left(1 - \frac{\omega_1^2}{\omega^2} n_{f21}^2\right)\hat{I}_3 \\ &\quad + k_{24}\sqrt{\frac{L_4}{L_3}}\hat{I}_4 \\ 0 &= k_{14}\sqrt{\frac{L_1}{L_4}}\hat{I}_1 + k_{24}\sqrt{\frac{L_2}{L_4}}\hat{I}_2 + k_{34}\sqrt{\frac{L_3}{L_4}}\hat{I}_3 \\ &\quad + \left(1 - \frac{\omega_1^2}{\omega^2} + R_{L,\mathrm{eq}}\right)\hat{I}_4 \end{aligned} \tag{2}$$

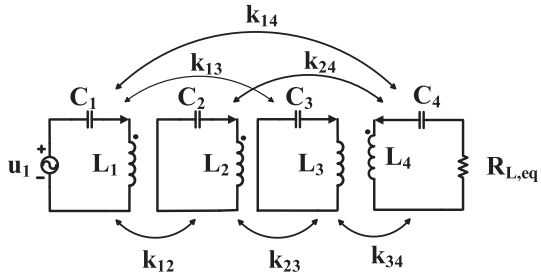

Fig. 3. Equivalent circuit of the proposed four-coil WPT system.

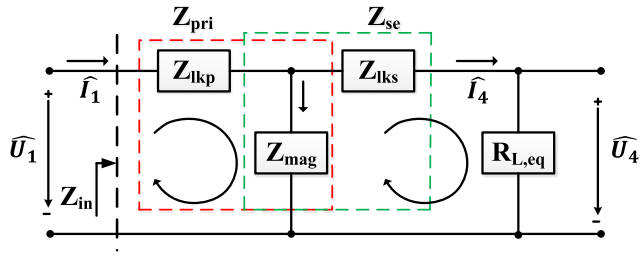

Fig. 4. Two port impedance network of the proposed WPT system.

where n_{f21} is the ratio of the resonant frequency of coil 1 and coil 2 (f_2/f_1); L_1, L_2, L_3, and L_4 are the self-inductances of the coils; and $k_{12}, k_{13}, k_{14}, k_{23}, k_{24}$, and k_{34} are the coupling coefficients between the two coils as shown in Fig. 3. In order to facilitate the analysis, it is assumed that the parameters of the primary side are the same as those of the secondary side ($L_1 = L_4$, $L_2 = L_3$, $k_{12} = k_{34}$, and $k_{13} = k_{24}$). Here, each coil has its resonant frequency at $f = \frac{1}{2\pi\sqrt{LC}}$, and the coil resistance is neglected since the most of the voltage is applied to the coil inductance.

The proposed WPT system can now be represented by a two-port impedance network as shown in Fig. 4, and the two closed-loop voltage equations can be obtained as

$$\begin{aligned} \hat{U}_1 &= \hat{I}_1 Z_{\mathrm{pri}} - \hat{I}_4 Z_{\mathrm{mag}} \\ 0 &= \hat{I}_1 Z_{\mathrm{mag}} - \hat{I}_4 (Z_{\mathrm{se}} + R_{L,\mathrm{eq}}) \end{aligned} \tag{3}$$

where Z_{mag} is the effective magnetizing impedance between the transmitter and receiver, Z_{pri} and Z_{se} are the impedances of the transmitter and receiver, respectively, and ω is the operating frequency. The primary and secondary side impedances and the effective magnetizing impedance can be derived as

$$\begin{aligned} Z_{\mathrm{pri}} &= Z_{\mathrm{se}} = j\omega L_1 \\ &\times \left\{ 1 - \frac{\omega_1^2}{\omega^2} - \frac{\left(\kappa_{12}^2 + \kappa_{13}^2\right)\left(1 - \frac{\omega_1^2}{\omega^2} n_{f21}^2\right) - 2\kappa_{12}\kappa_{13}\kappa_{23}}{\left(1 - \frac{\omega_1^2}{\omega^2} n_{f21}^2\right)^2 - \kappa_{23}^2} \right\} \\ Z_{\mathrm{mag}} &= j\omega\sqrt{L_1 L_4} \\ &\times \left\{ \kappa_{14} - \frac{2\kappa_{12}\kappa_{13}\left(1 - \frac{\omega_1^2}{\omega^2} n_{f21}^2\right) - \kappa_{23}\left(\kappa_{12}^2 + \kappa_{13}^2\right)}{\left(1 - \frac{\omega_1^2}{\omega^2} n_{f21}^2\right)^2 - \kappa_{23}^2} \right\}. \end{aligned} \tag{4}$$

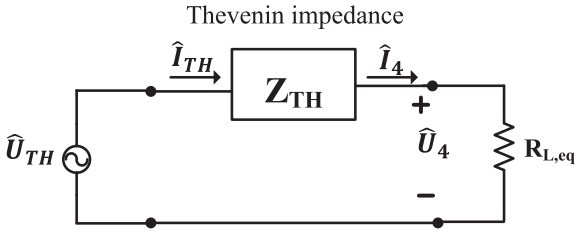

Fig. 5. Thevenin equivalent circuit of the proposed WPT system.

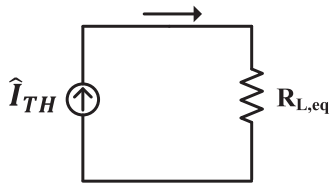

Fig. 6. Thevenin equivalent circuit of the proposed system to achieve CC mode charge when $Z_{\rm pri} = 0$.

The derivation procedure can be found in Appendix A1.

B. Implementation of the CC/CV Mode Charge With the Proposed WPT System

As mentioned above, the CC and CV mode charges can be implemented by operating the converter as a current source and as a voltage source. This can be achieved by suitably designing the compensation network. The two port impedance network of the proposed WPT system in Fig. 4 can be further simplified by using Thevenin theorem as shown in Fig. 5. The equations for the Thevenin equivalent circuit can be derived as

$$\hat{U}_{\rm TH} = \hat{U}_1 \frac{Z_{\rm mag}}{Z_{\rm pri}} \tag{5}$$

$$Z_{\rm TH} = \frac{Z_{\rm pri} Z_{\rm se} - Z_{\rm mag}^2}{Z_{\rm pri}} = \frac{Z_{\rm pri}^2 - Z_{\rm mag}^2}{Z_{\rm pri}} \tag{6}$$

$$\hat{I}_{\rm TH} = \frac{\hat{U}_{\rm TH}}{Z_{\rm TH} + R_{L,\rm eq}} = \frac{\hat{U}_1 Z_{\rm mag}}{Z_{\rm pri}^2 - Z_{\rm mag}^2 + Z_{\rm pri} R_{L,\rm eq}} \tag{7}$$

$$\hat{U}_4 = \frac{\hat{U}_{\rm TH} R_{L,\rm eq}}{Z_{\rm TH} + R_{L,\rm eq}} = \hat{U}_1 \frac{Z_{\rm mag} R_{L,\rm eq}}{Z_{\rm pri}^2 - Z_{\rm mag}^2 + Z_{\rm pri} R_{L,\rm eq}} \tag{8}$$

where $\hat{U}_{\rm TH}$ and $Z_{\rm TH}$ represent the Thevenin impedance and Thevenin voltage of the proposed circuit, respectively. It can be easily deduced from (7), (8), and Fig. 5 that it is possible to implement the CC and CV mode charges by making $|\hat{I}_{\rm TH}|$ and $|\widehat{U_4}|$ constant regardless of $R_{L,\rm eq}$.

It can be easily noticed from (7) that the Thevenin current $|\hat{I}_{\rm TH}|$ is almost constant regardless of the load if the Thevenin impedance $Z_{\rm TH}$ is designed to have a larger value than that of $R_{L,\rm eq}$. It can be achieved by making $Z_{\rm pri}$ in (7) equal to 0 at the operating frequency as shown in (9). Since the Thevenin impedance $Z_{\rm TH}$ and the Thevenin voltage $|\hat{U}_{\rm TH}|$ both become almost infinite under this condition, the CC mode charge can be implemented as shown in Fig. 6. The output current gain curves with respect to the frequency at variable loads are shown

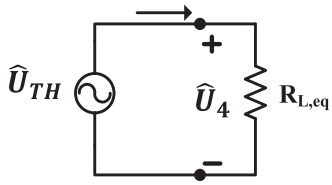

Fig. 7. Thevenin equivalent circuit of the proposed system to achieve CV mode charge when $Z_{\rm pri}^2 - Z_{\rm mag}^2 = 0$.

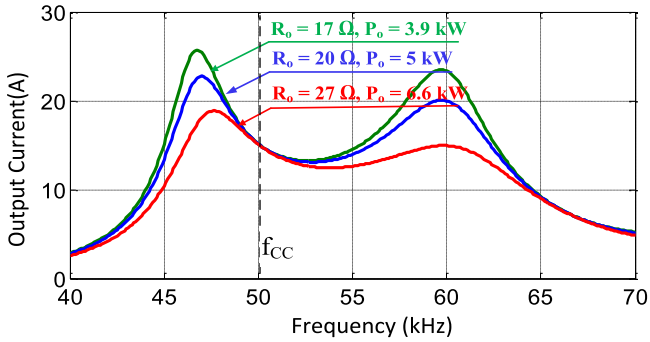

Fig. 8. Output current curves of the proposed system at different loads in CC mode operation.

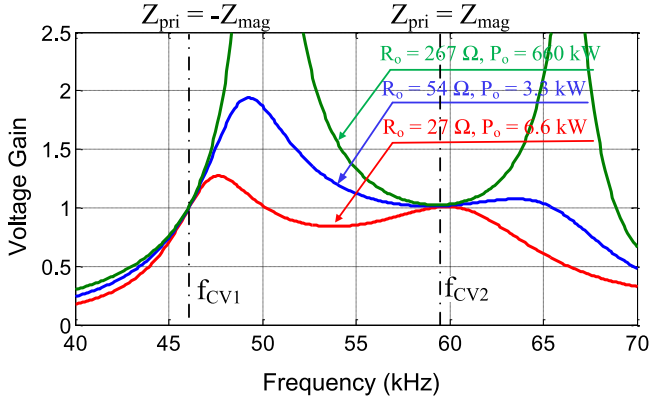

Fig. 9. Voltage gain curves of the proposed system at different loads.

in Fig. 8 to verify the aforementioned analysis. As shown in Fig. 8. It can be seen that the CC mode charge with 15.7 A can be implemented at 50 kHz. In addition, since $Z_{\rm pri} = Z_{\rm se}$ from (4), the input impedance $Z_{\rm in}$ of the system becomes a real number as shown in (10). Hence, the ZPA condition can be obtained in the CC mode charge

$$\hat{I}_{\rm TH} = -\frac{\hat{U}_1}{Z_{\rm mag}}, \text{if} Z_{\rm pri} = 0 \tag{9}$$

$$Z_{\rm in} = Z_{\rm pri} - Z_{\rm mag} + \frac{(Z_{\rm se} - Z_{\rm mag} + R_{L,\rm eq}) Z_{\rm mag}}{Z_{\rm se} + R_{L,\rm eq}} = \frac{-Z_{\rm mag}^2}{R_{L,\rm eq}}. \tag{10}$$

The voltage gain curves of the proposed WPT system with respect to the frequency with variable loads are drawn by using (8) and shown in Fig. 9. It can be also noticed from (8) and

Fig. 7 that it is possible to make the output voltage $|\hat{U}_4|$ constant regardless of the load if the Thevenin impedance $Z_{\rm TH}$ is equal to zero. It can also be seen in Fig. 9 that there are two different resonant frequencies at which the CV mode can be implemented.

The Thevenin impedance in (6) becomes zero if $Z_{\rm pri}^2 - Z_{\rm mag}^2 = 0$ at the resonant frequency. Then, the output voltage $|\hat{U}_4|$ is equal to $\hat{U}_{\rm TH}$ which makes it possible to implement the CV mode charge as shown in Fig. 7. In this case, the input impedance of the proposed system in (10) and its phase can be represented as

$$Z_{\rm in} = \frac{Z_{\rm pri} R_{L,\rm eq}}{Z_{\rm se} + R_{L,\rm eq}}, \arg\left[\frac{-R_{L,\rm eq}}{Z_{\rm mag}}\right]. \tag{11}$$

The derivation procedure for the phase of the input impedance in (11) can be found in Appendix A2.

It can be noticed from (11) that the input impedance of the system and its phase varies when the load varies. Hence, similar to the conventional converter, it does not seem possible to achieve the ZPA condition over the entire charge operation. However, it can be achieved in the proposed topology by designing an effective magnetizing impedance $Z_{\rm mag}$ that is very large. Unlike the conventional converter topology, it is possible to make it large due to the presence of two intermediate coils. A method to maximize the magnetizing impedance $Z_{\rm mag}$ is detailed in the following section.

C. *Efficiency Maximization of the Proposed WPT System During the CV Mode Charge by Achieving the ZPA Condition*

Typically, a WPT system consists of three major blocks, a full bridge inverter, a compensation network, and a diode rectifier. The efficiency of the system is primarily dependent upon the switching loss of the full bridge inverter and the effectiveness of the resonant tank in terms of power transfer. In order to obtain a higher efficiency, the proposed system needs to be designed to achieve the ZPA condition for soft switching. In the CC mode charge, this can be achieved naturally since the input impedance $Z_{\rm in}$ is a real number as shown in (10). Hence, it is only necessary to derive the condition to achieve it in the CV mode charge. As already mentioned in Section II–B, the CV mode charge can be implemented if following equation is satisfied:

$$\begin{cases} |Z_{\rm pri}| = |Z_{\rm mag}| \\ Z_{\rm mag} \approx \infty \end{cases} \tag{12}$$

The first condition in (12) implies that there is freedom in designing the impedance of the resonant tank to be $Z_{\rm pri} = Z_{\rm mag}$ or $Z_{\rm pri} = -Z_{\rm mag}$. It is necessary to investigate which provides the better results in operation. At first, the following equation can be derived by using (4) and (12) when $Z_{\rm pri} = Z_{\rm mag}$:

$$\begin{cases} 1 - \dfrac{\omega_1^2 n_{f21}^2}{\omega^2} - k_{14} + \dfrac{(k_{12}-k_{13})^2}{2k_{23}} = 0 \\ 1 - \dfrac{\omega_1^2 n_{f21}^2}{\omega^2} + k_{23} = 0. \end{cases} \tag{13}$$

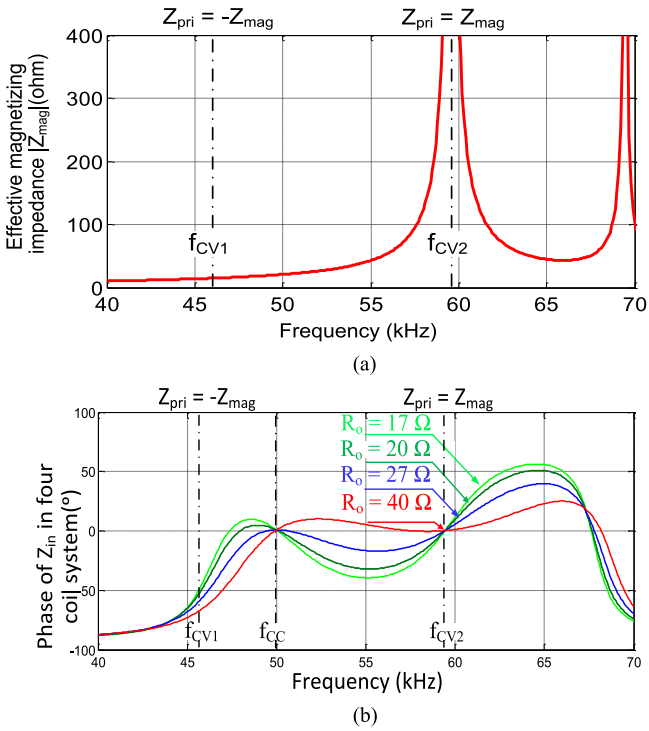

Fig. 10. Characteristic curves of the proposed converter if ZPA condition is achieved at $f_{\rm CV2}$ (a) effective magnetizing impedance $Z_{\rm mag}$ and (b) phase of input impedance $Z_{\rm in}$.

Therefore, the ratio of the resonant frequency of coil 1 and coil 2 n_{f21} can be represented as

$$n_{f21} = \sqrt{\frac{1+k_{23}}{1-k_{14}+\frac{(k_{12}-k_{13})^2}{2k_{23}}}}. \tag{14}$$

It is shown in (14) that if the resonant frequency ratio n_{f21} satisfies the relationship in (14), the ZPA condition can be achieved in the CV mode charge. This also means that the proposed WPT converter can operate under the full soft switching condition during the CV mode charge.

Fig. 10 is drawn with (4) and (11) to show the phase of the input impedance $Z_{\rm in}$ and the magnitude of the effective magnetizing impedance $Z_{\rm mag}$ at different loads. As shown in Fig. 10(a), the ZPA condition is achieved at the frequency $f_{\rm CV2}$ since the effective magnetizing impedance is very large. Hence, the phase of $Z_{\rm in}$ is almost zero regardless of the load. However, at the frequency $f_{\rm CV1}$, due to the small effective magnetizing impedance, the ZPA condition cannot be achieved as shown in Fig. 10(b).

Similarly, when $Z_{\rm pri} = -Z_{\rm mag}$, then the ratio of the resonant frequency of coil 1 and coil 2 n_{f21} can be represented as

$$n_{f21} = \sqrt{\frac{1-k_{23}}{1+k_{14}-\frac{(k_{12}+k_{13})^2}{2k_{23}}}}. \tag{15}$$

Fig. 11 shows the phase of the input impedance $Z_{\rm in}$ and the magnitude of the effective magnetizing impedance $Z_{\rm mag}$ when (15) is satisfied. Unlike the previous case, the ZPA condition is

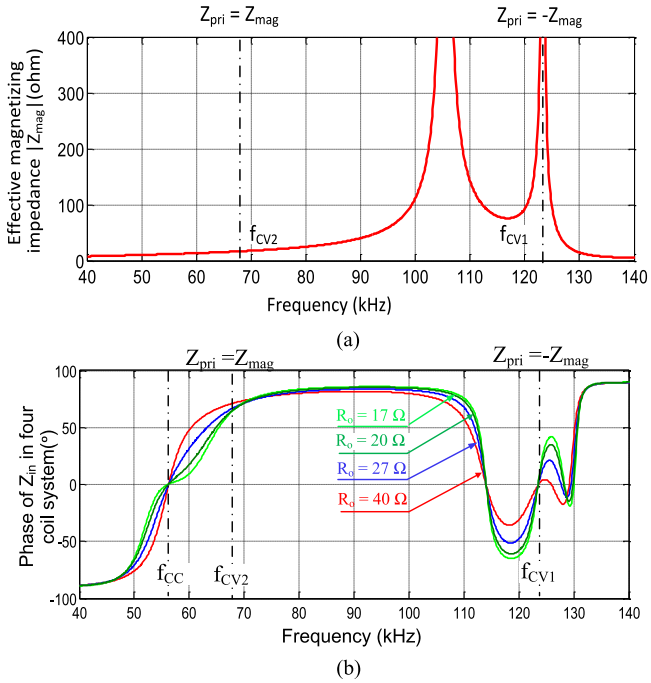

Fig. 11. Characteristic curves of the proposed converter if ZPA condition is achieved at f_{CV1} (a) effective magnetizing impedance Z_{mag} and (b) phase of input impedance Z_{in}.

achieved at the frequency f_{CV1} since the effective magnetizing impedance is very large at this frequency. However, the range of the frequency f_{CC} and f_{CV1} between the CC and CV mode charges in this case is a lot wider than that of the first case. This makes it difficult to optimize the WPT system. Therefore, the resonant frequency ratio n_{f21} calculated with (14) is selected to design the resonant tank to achieve the CV mode charge.

III. Design of the Resonant Tank

In order to implement the CC/CV charge with the proposed four-coil system it is crucial to suitably design the resonant tank. However, owing to the complication of the input parameters, the design of the resonant tank should be performed carefully according to the order of sequence. In this section the detail design procedure for a 6.6 kW WPT system with a 200 mm air gap is presented step by step to provide an effective design guide. In this design, the planar spiral coil is selected since it is able to create a higher magnetic coupling for a given area when compared to the other types such as rectangular or square coils [5].

A. Design of the Inductance of Transmitter and Receiver Coil

The first step of the design procedure for a four-coil resonator system is to determine the self-inductance of the transmitter and receiver coils. Here, an initial guess for the number of turns of the coil is required to determine the optimal number of turns of the coil by the trial-and-error method. Typically, the diameter of the transmitter coil is chosen to be less than four times the airgap distance [5]. Hence, a suitable initial guess for the number of turns is selected under this geometric limitation. Since a higher magnetic coupling is always desirable for higher power transfer efficiency, the resonators need to be designed to have higher coupling coefficients. In addition, a larger quality factor is desirable in order to reduce the conduction loss caused by the resistance of the coil. Here, it should be noted that the actual turn ratio between the transmitter and receiver coils needs to be taken into account by using [5]

$$\frac{U_o}{U_{\mathrm{dc}}} \approx \sqrt{\frac{L_4}{L_1}}. \tag{16}$$

Based on the limitations mentioned above, the optimal number of turns which gives the highest coupling coefficients can be found based on the iterations.

B. Design of the Inductance Values of Intermediate Coils

The second step is to decide the self-inductance value of the intermediate coils. In order to minimize the conduction loss of the intermediate coil, it is desirable for the quality factor to be 500–600 [15]. Again, an initial guess for the number of turns of the intermediate coil is used to determine the optimal value to maximize the quality factor by the trial-and-error method

$$L_2 = \frac{r_2 Q_2}{2\pi f} \tag{17}$$

$$L_3 = \frac{r_3 Q_3}{2\pi f} \tag{18}$$

where r_2 and r_3 are the ac resistances of intermediate coils 2 and 3, respectively. Q_2 and Q_3 are the quality factors of intermediate coils 2 and 3, respectively.

C. Determination of the Resonant Frequency of the Transmitter and Intermediate Resonators

The resonant frequency of the transmitter coil $f_1 = \frac{1}{2\pi\sqrt{L_1 C_1}}$ can be determined by using some equations when the converter is operating in the CC mode. By using (1) and (9), the effective magnetizing impedance can be represented as

$$Z_{\mathrm{mag}} = \frac{|\hat{U}_1|}{|\hat{I}_4|} = \frac{8U_{\mathrm{dc}}}{\pi^2 I_o}. \tag{19}$$

By substituting (4) into (19), we get

$$\frac{8U_{\mathrm{dc}}}{\pi^2 I_o} = \left| j\omega\sqrt{L_1 L_4} \left\{ \kappa_{14} - \frac{2\kappa_{12}\kappa_{13}\left(1 - \frac{\omega_1^2}{\omega^2} n_{f21}^2\right) - \kappa_{23}\left(\kappa_{12}^2 + \kappa_{13}^2\right)}{\left(1 - \frac{\omega_1^2}{\omega^2} n_{f21}^2\right)^2 - \kappa_{23}^2} \right\} \right|. \tag{20}$$

Since the operating frequency in the CC mode charge is 50 kHz, as shown in Fig. 8, the resonant frequency f_1 of the intermediate coil in (20) can be solved by a numerical method. The resonant frequency f_2 of the intermediate coil can then be easily calculated by using n_{f21} as

$$f_2 = f_1 * n_{f21}. \tag{21}$$

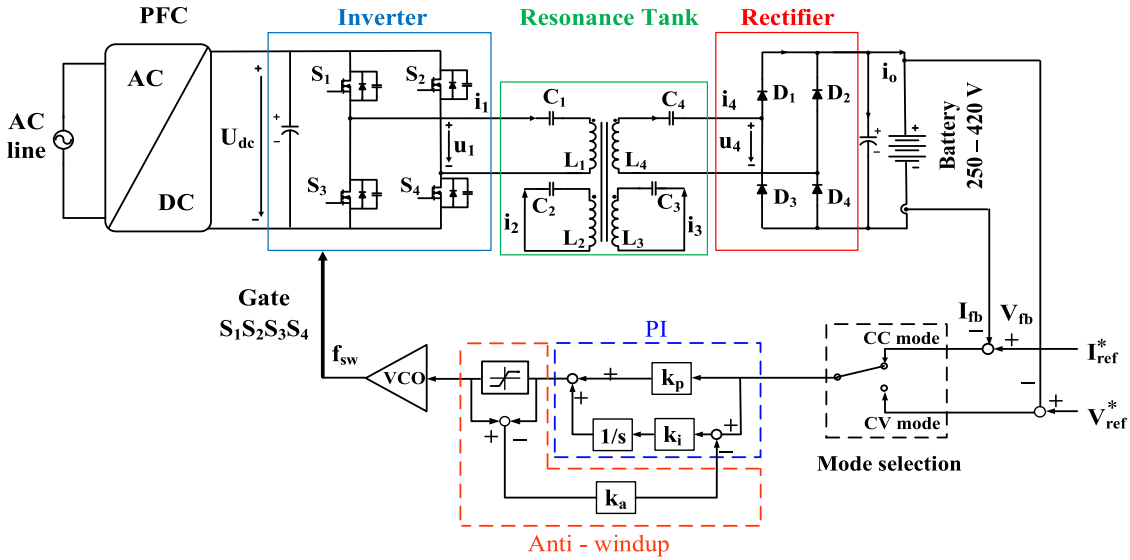

Fig. 12. Closed-loop control structure of the proposed four-coil wireless on-board charger system.

D. Determination of the Resonant Capacitance Value

After the inductances of the four-coils and their resonant frequencies are determined, then the resonant capacitance values C_1, C_2, C_3, and C_4 can be calculated as

$$C_1 = \frac{1}{\omega_1^2 L_1}, C_2 = \frac{1}{\omega_2^2 L_2}, C_3 = \frac{1}{\omega_2^2 L_3}, C_4 = \frac{1}{\omega_1^2 L_4}. \quad (22)$$

IV. Design of the Closed Loop Controller for the CC/CV Charge

Once the resonant tank is suitably designed according to the design procedure presented in Section III, the CC and CV mode charges can be simply implemented at each fixed resonant frequency while achieving the ZPA and the full soft switching condition. However, it is only possible under the assumption that the output voltage of the front-end PFC converter is always constant. Hence, the operation of the WPT converter deviates slightly from the perfect resonant condition if the output voltage of the front-end PFC converter is not constant. It may vary due to variations in the ac input to the PFC converter. Therefore, closed-loop control is necessary to achieve the CC and CV mode charge operations while maintaining the ZPA and soft switching conditions under input voltage variations. A simple PI control scheme is adopted as shown in Fig. 12. The controller is composed of a PI controller, a mode transfer switch, a limiter, an anti-wind-up scheme, and a voltage-controlled oscillator. Since each mode of the control requires its own independent controller, one of two is selected by the transfer switch according to the mode of charge. The limiter is used to prevent the converter from operating at lower frequencies than the frequency at which the peak voltage gain is obtained with a maximum load (6.6 kW) so that the WPT converter can always operate in the inductive region. The anti-wind-up scheme is adopted to reduce the overshoot and transient time caused by the limiter operation.

When the battery voltage is lower than the maximum charge voltage, 420 V in this research, the current controller is activated to charge the battery with the CC mode. Once the voltage of the battery reaches its maximum charge voltage, the controller automatically switches its mode to the CV mode charge.

To design the PI controllers, open loop transfer functions for each mode of operation are obtained by using the ac sweep function in power electronics simulation (PSIM) software as shown in Fig. 13. Fig. 13(a) and (b) shows bode plots for the current control and voltage control under different load conditions, respectively. The PI controller for each mode of charge is designed to provide enough of a phase margin at the crossover frequency. The bandwidth and phase margin of the current controller are 850 Hz and 60°, respectively

$$G_{\mathrm{ci}}(s) = 0.0015 + \frac{21}{s}. \quad (23)$$

Similarly, the bandwidth and phase margin of the voltage controller are 100 Hz and 90°, respectively

$$G_{\mathrm{cv}}(s) = 0.0001 + \frac{3}{s}. \quad (24)$$

V. Experimental Results

Based on the previous analysis and design, a 6.6 kW WPT system is implemented to verify the proposed design method. All of the parameters for the resonant tank are shown in Table II. The airgap between the primary side and secondary side is set to 200 mm since the mounting distance for common passenger cars is known to be 150–300 mm. Fig. 14 shows the implemented coils for the proposed WPT system with a 200 mm air gap. Two intermediate resonators are placed inside the transmitter and receiver coil. In order to implement the resonant tank, film capacitors are used. The resonant capacitors are arranged in an array form to meet the voltage and current ratings and to get better heat dissipation. In the proposed system, four MOSFETs

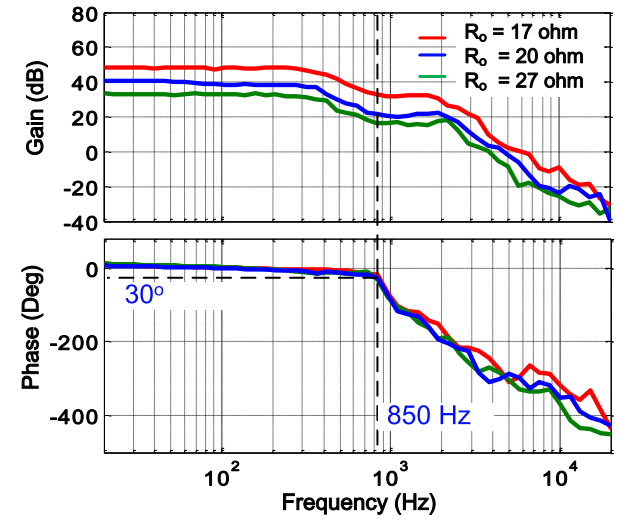

(a)

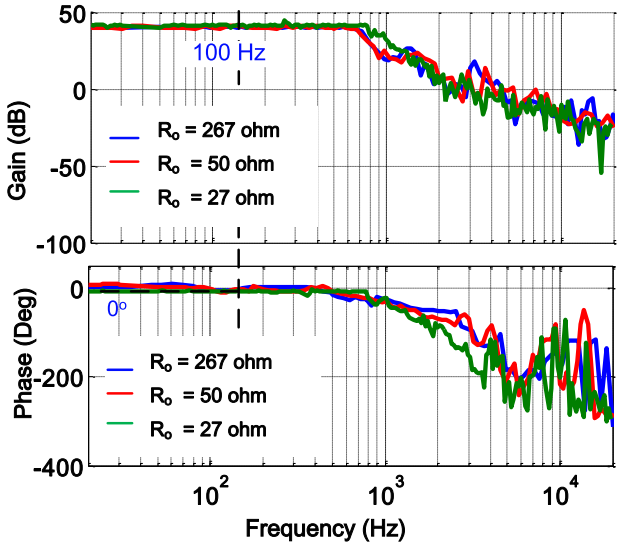

(b)

Fig. 13. Bode plots of the proposed converter at different loads: (a) CC mode operation at 50 kHz; and (b) CV mode operation at 59.5 kHz.

TABLE II
PARAMETERS FOR THE RESONANT TANK

Parameters	Designed Par.	Measured Par.
Self-inductance L_1	132 μH	132.4 μH
Self-inductance L_2	80 μH	79.7 μH
Self-inductance L_3	98 μH	98.3 μH
Self-inductance L_4	135 μH	135.6 μH
Resonance Cap C_1	56.78 nF	56.76 nF
Resonance Cap C_2	75.1 nF	75.76 nF
Resonance Cap C_3	64.15 nF	64.12 nF
Resonance Cap C_4	54.54 nF	54.51 nF

(IXFB120N50P2) and four diodes (DSEI120-06A) are used to implement the inverter.

Fig. 15 shows experimental waveforms of the proposed converter in both the CC and CV mode charges at 6.6 and 3.3 kW of output power, respectively. Here, I_1 and I_4 are the currents at the transmitter and receiver coil, and I_2 and I_3 are the currents at

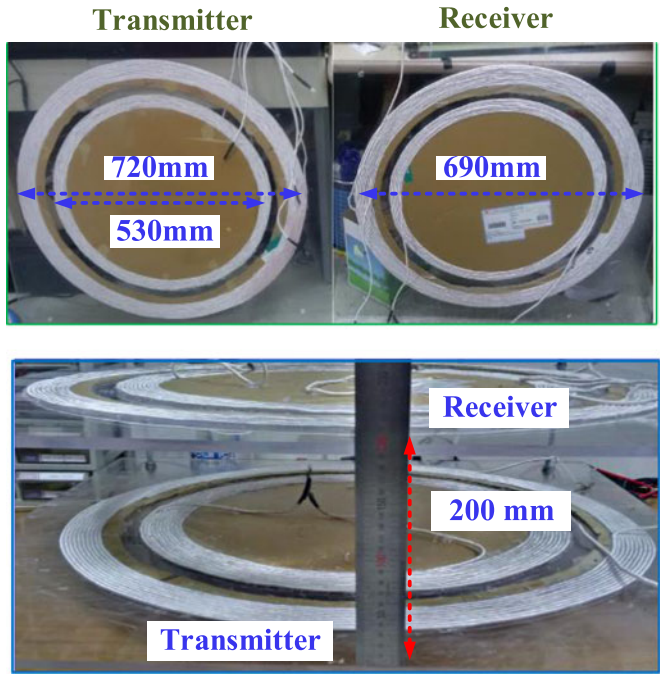

Fig. 14. Implemented coils for the proposed WPT system.

the intermediate coils, respectively. U_1 and U_4 are the voltages at the input and output of the resonant tank. It can be seen from Fig. 15(a) and (b) that MOSFET S_4 turns ON with zero-voltage switching (ZVS) and turns OFF with nearly zero-current switching (ZCS) in both cases. It can be also seen from Fig. 15 that the rectifier diode D_1 in the secondary side achieves perfect soft switching. Therefore, the proposed WPT system can achieve a rather high efficiency.

In Fig. 16, the prototype of the proposed WPT converter and the thermal images of the WPT coils, MOSFETs, and diode are shown. As shown in Fig. 16, the temperature of each component is maintained at a reasonable value. Since, the proposed WPT system operates at almost a fixed resonant frequency in each CC and CV mode, the circulating current can be minimized. The main loss of the coils is only the conduction loss and it is quite small in case of Litz wire due to its lower resistance value. Therefore, the temperature of the coils can be maintained at a low value (34.1 °C at 6.6kW) as shown in Fig. 16(b).

Typically, the switching loss is a major portion of the losses at the switches of the converters. In the proposed WPT converter, the full ZVZCS condition in MOSFET switches can be achieved over the wide range of load. As a result, the loss at the switch can be minimized and hence the temperature rise of the MOSFETs can be limited around 40 °C with full load as shown in Fig. 16(c).

In the meanwhile, since the conduction loss is the major portion of the losses at the diodes, the maximum temperature of the diode reaches 52 °C due to the high rms current as shown in Fig. 16(d).

Fig. 17(a) and (b) shows the dynamic responses of the WPT system when the power reference has a step change from 3.9 to 4.8 kW in the CC mode charge, and when the current reference has a step change from 3.9 to 2.9 kW in the CV mode charge. The transition time is about 16 ms in the CC mode and about

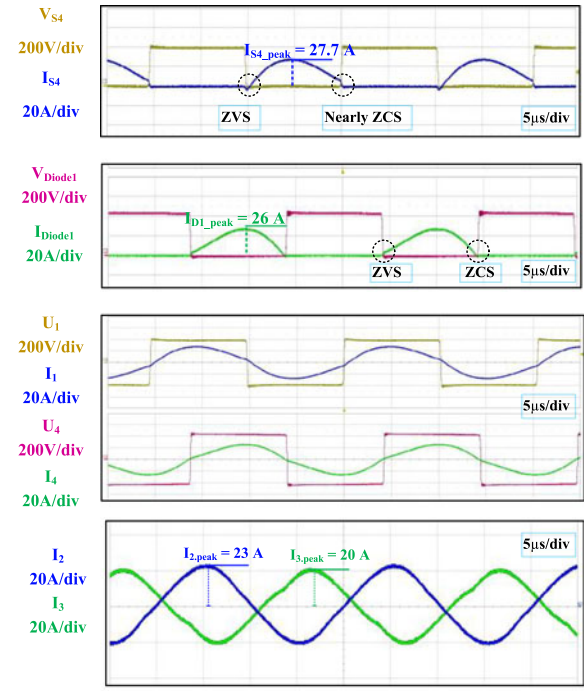

Fig. 15. Key waveforms of the proposed WPT converter in both CC and CV mode charge: (a) at 6.6 kW in CC mode; and (b) at 3.3 kW in CV mode.

20 ms in the CV mode, which is good enough for battery charge applications.

Fig. 18 shows the efficiency of the proposed WPT system in both the CC and CV mode charge operations. The maximum efficiency is 97.08% at 3.7 kW in the CV mode and 96.39% at 6.1 kW in the CC mode.

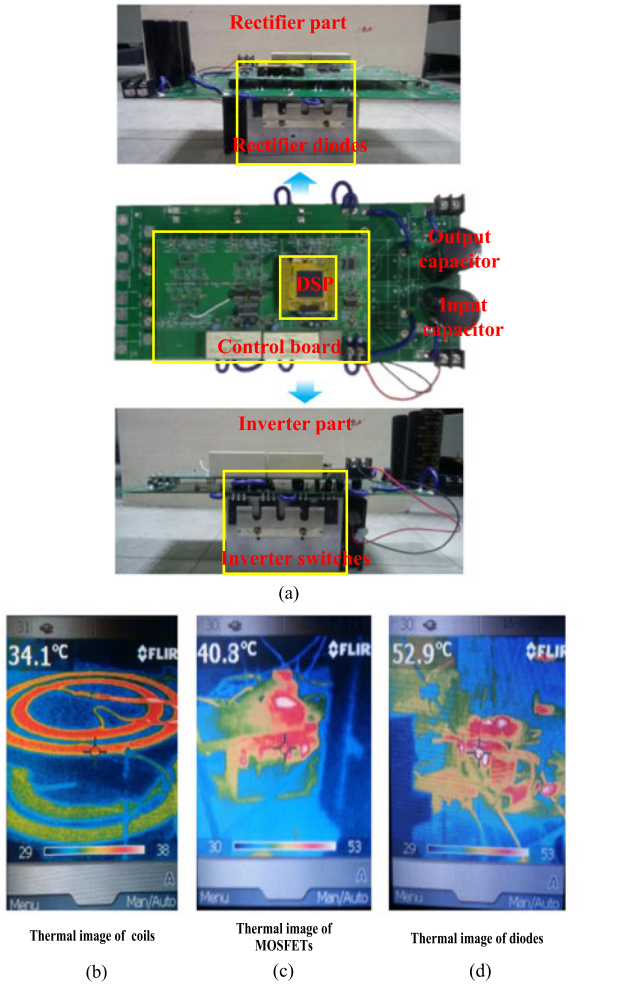

Fig. 16. Prototype of the proposed WPT converter and thermal images of each component in the proposed WPT system at 6.6 kW.

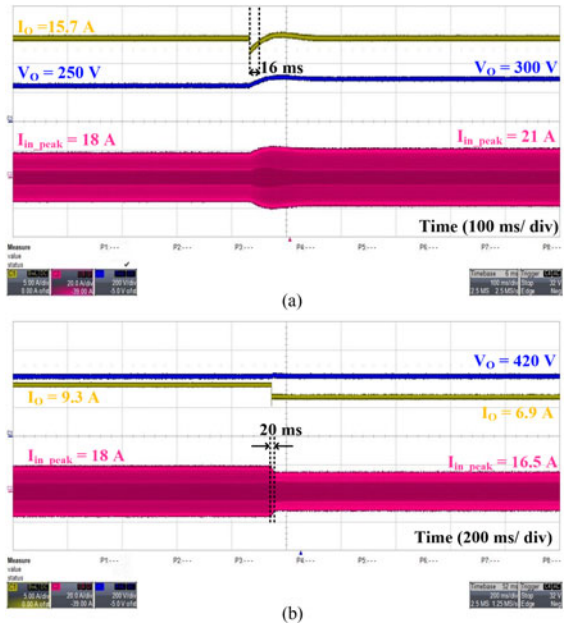

Fig. 17. Dynamic response of the closed-loop WPT system (a) CC mode at 50 kHz when P_o changes from 3.9 to 4.8 kW ($I_o = 15.7$ A) and (b) CV mode at 59.4 kHz when P_o changes from 3.9 to 2.9 kW ($V_o = 420$ V).

TABLE III
COMPARISON OF VARIOUS WPT TOPOLOGIES

	WPT with two coils			WPT with three coils	WPT with four coils		
	Ref. [5]	Ref. [11]	Ref. [9]	Ref. [17]	Ref. [19]	Ref. [21]	Proposed
Power	5.5 kW	8 kW	22 kW	6.6 kW	3.3 kW	3.3 kW	6.6 kW
Shape of the coil	Circular	Rectangular	Rectangular	Rectangular	Rectangular	Rectangular	Circular
Size of the transmitter coil (mm)	210	600 × 600	800 × 600	800 × 800	800 × 800	575 × 575	720
Size of the receiver coil (mm)	210	600 × 600	800 × 600	600 × 600	600 × 600	575 × 575	690
Size of the intermediate coil (mm)	N/A	N/A	N/A	400	Int.1: 400 Int.2: 300	Int.1: 390 Int.2: 390	Int.1: 520 Int.2: 520
Operating frequency (kHz)	100	95	20	100	90	100	60
Distance between coils (mm)	50	150	200	200	200	210	200
Use of Ferrite core	Yes	Yes	Yes	No	No	Yes	No
Switching characteristics in CC mode	ZVS Turn-ON	ZVS Turn-ON	ZVS Turn-ON	Hard switching turn-ON	Hard switching turn-ON	ZVS Turn-ON	ZVS Turn-ON
	ZCS Turn-OFF	ZCS Turn-OFF	ZCS Turn-OFF	ZCS Turn-OFF	ZCS Turn-OFF	Hard switching Turn-OFF	ZCS Turn-OFF
Switching characteristics in CV mode	ZVS Turn-ON	ZVS Turn-ON	ZVS Turn-ON	ZVS Turn-ON	ZVS Turn-ON	ZVS Turn-ON	ZVS Turn-ON
	Hard switching Turn-OFF	Hard switching Turn-OFF	Hard switching Turn-OFF	Hard switching Turn-OFF	Hard switching Turn-OFF	Hard switching Turn-OFF	ZCS Turn-OFF
ZPA condition	CC mode	CC mode	CC mode	CV mode	CV mode	N/A	CC mode CV mode
Req. for additional converter	Yes	Yes	Yes	Yes	Yes	Yes	No
Maximum Efficiency (%)	96.5	95.36	95	96	96.56	92	97.1

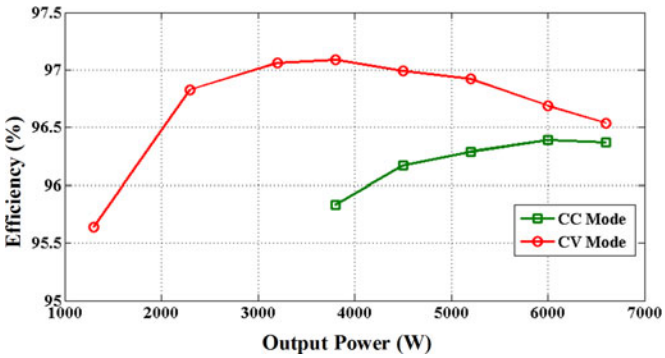

Fig. 18. Efficiency of the proposed four-coil WPT system.

TABLE IV
VARIATION OF THE COUPLING COEFFICIENTS IN MISALIGNMENT CONDITIONS

Coupling coefficient	Perfect alignment	Vertical misalignment (10 cm)	Lateral misalignment (20 cm)
k_{12}	0.396	0.396	0.396
k_{13}	0.15	0.096	0.113
k_{14}	0.213	0.141	0.12
k_{23}	0.155	0.073	0.05
k_{24}	0.17	0.097	0.115
k_{34}	0.385	0.385	0.385

In order to show the superiority of the proposed four coil WPT converter topology, the performance of the proposed converter has been compared with the various WPT converter topologies as shown in Table III. It can be concluded from Table III that the proposed converter is superior to the other topologies in terms of efficiency.

In practical EV applications, it is difficult to assume that the charge is always performed with the coils aligned perfectly. Hence, it is required to verify the performance of the WPT system when there is a misalignment in between the transmitter and receiver coils. Two kinds of misalignment tests, vertical misalignment and lateral misalignment, have been conducted and the waveforms and efficiencies at each condition are presented. As well known, the efficiency of the WPT system under the coil misalignment degrades. In the experiments, the system is configured to have a vertical misalignment in the range of 0–10 cm (the transmission distance between the source coil and the load coil is in range of 20–30 cm) and a lateral misalignment in the range of 0–20 cm at 3.4 kW in CV mode. In order to maintain the output power constant under various misalignment conditions, the operating frequency of the system is adjusted.

Table IV shows the variation of the coupling coefficients of the coils when the receiver coil is misaligned from the transmitter coils. The longer the misalignment distance, the lower the coupling factor.

Fig. 19 shows the experimental results to verify the performance of the proposed WPT converter under misalignment conditions. Fig. 19(a) shows the voltage and current waveforms of the proposed converter under perfect misalignment and the

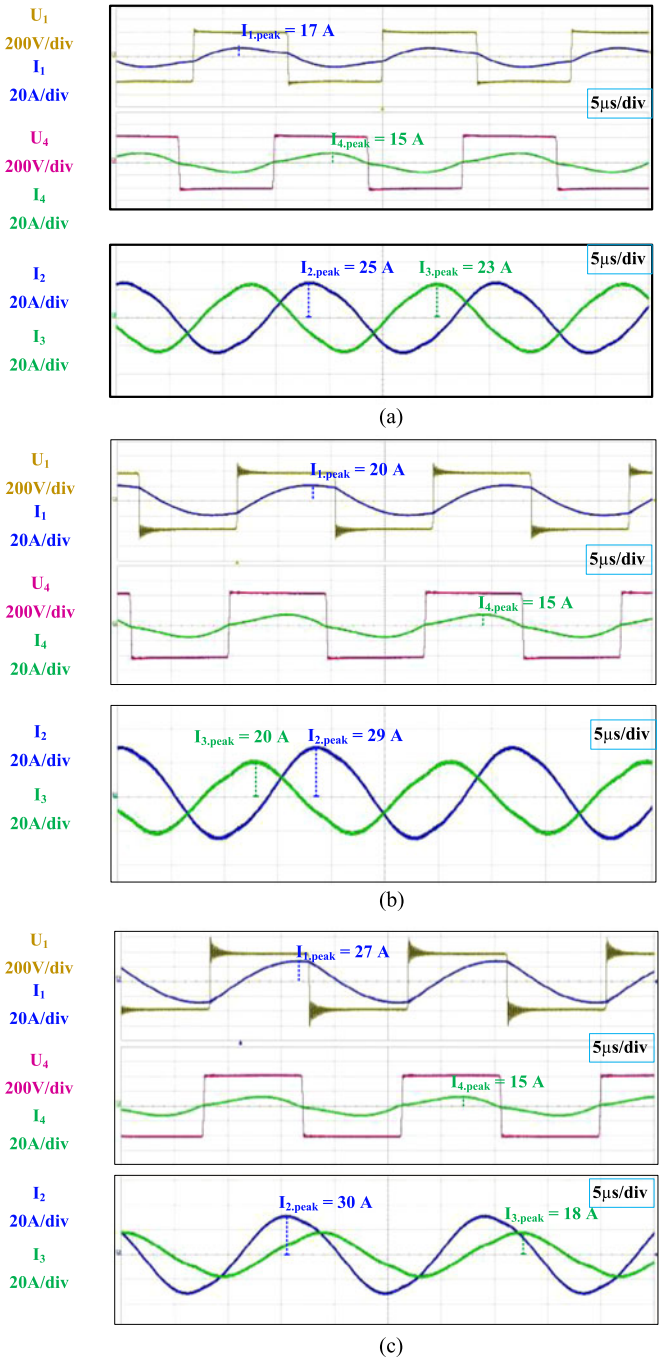

Fig. 19. Voltage and current waveforms of the proposed converter under various misalignment conditions. (a) Perfect alignment. (b) Lateral misalignment (20 cm). (c) Vertical misalignment (10 cm).

switching frequency is 59.5 kHz. Fig. 19(b) shows the voltage and current waveforms of the proposed converter under the 20 cm lateral misalignment. In this case, the switching frequency is adjusted from 59.5 to 56 kHz to regulate the output voltage and the proposed WPT system operates in the inductive region. Fig. 19(c) shows the voltage and current waveforms under the 10 cm vertical misalignment. In this case, the switching frequency is adjusted from 59.5 to 56.5 kHz to regulate the output voltage. The nonzero phase of input impedance leads to a hard switching operation of the MOSFET with large turn-OFF current

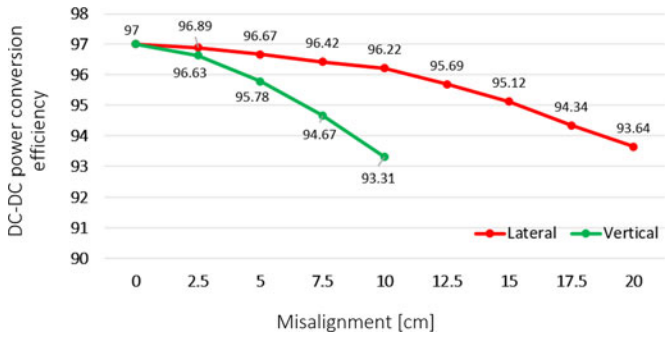

Fig. 20. Efficiency of the proposed WPT converter under various misalignment conditions.

and increases the magnitude of the currents in transmitter and intermediate coils. As a result, the efficiency of the system is decreased. In case of 10 cm vertical misalignment and 20 cm lateral misalignment, the efficiency of the proposed converter is 93.31% and 93.64%, respectively, as shown in Fig. 20.

VI. Conclusion

In this paper, a high-efficiency WPT system with intermediate coils is introduced and its feasibility and validity has been demonstrated by a 6.6-kW prototype circuit. High efficiency of the proposed converter can be obtained by the improved coupling factors with the help of two additional intermediate coils. It is possible for the proposed converter to achieve the ZPA condition and soft switching in both the CC and CV modes over the entire charge operation. In addition, the proposed WPT system can implement the CC and CV mode charges at a fixed resonant frequency. A peak efficiency of 97.08% at 3.7 kW with a 200 mm airgap has been achieved.

Appendix

A. Derivation Procedure for the Primary Side Impedance $Z_{\rm pri}$, Secondary Impedance $Z_{\rm se}$, and Effective Magnetizing Impedance $Z_{\rm mag}$

Here, the derivation procedure for the primary, secondary, and effective magnetizing impedances of the proposed WPT with (A1) is presented. As already mentioned above, the voltage equations of the circuit can be represented as

$$\frac{\hat{U}_1}{j\omega L_1} = \left(1-\frac{\omega_1^2}{\omega^2}\right)\hat{I}_1 + k_{12}\sqrt{\frac{L_2}{L_1}}\hat{I}_2 + k_{13}\sqrt{\frac{L_3}{L_1}}\hat{I}_3 + k_{14}\sqrt{\frac{L_4}{L_1}}\hat{I}_4$$

$$0 = k_{12}\sqrt{\frac{L_1}{L_2}}\hat{I}_1 + \left(1-\frac{\omega_1^2}{\omega^2}n_{f21}^2\right)\hat{I}_2 + k_{23}\sqrt{\frac{L_3}{L_2}}\hat{I}_3 + k_{24}\sqrt{\frac{L_4}{L_2}}\hat{I}_4$$

$$0 = k_{13}\sqrt{\frac{L_1}{L_3}}\hat{I}_1 + k_{23}\sqrt{\frac{L_2}{L_3}}\hat{I}_2 + \left(1-\frac{\omega_1^2}{\omega^2}n_{f21}^2\right)\hat{I}_3$$

$$+\ k_{24}\sqrt{\frac{L_4}{L_3}}\hat{I}_4$$

$$0 = k_{14}\sqrt{\frac{L_1}{L_4}}\hat{I}_1 + k_{24}\sqrt{\frac{L_2}{L_4}}\hat{I}_2 + k_{34}\sqrt{\frac{L_3}{L_4}}\hat{I}_3 + \left(1-\frac{\omega_1^2}{\omega^2}+R_{L,\mathrm{eq}}\right)\hat{I}_4. \quad \text{(A1)}$$

In order to derive the relationship between the input and the output, the variables of the intermediate coils need to be eliminated. With the top second equation of (A1), the current $\widehat{I_2}$ can be represented as

$$\hat{I}_2 = -\frac{\hat{I}_1 k_{12}\sqrt{\frac{L_1}{L_2}} + \hat{I}_3 k_{23}\sqrt{\frac{L_3}{L_2}} + \hat{I}_4 k_{24}\sqrt{\frac{L_4}{L_2}}}{1-\frac{\omega_1^2}{\omega^2}n_{f21}^2}. \quad \text{(A2)}$$

By substituting (A2) into (A1), (A1) can be rewritten as

$$\frac{\widehat{U_1}}{j\omega L_1} = \left(1-\frac{\omega_1^2}{\omega^2}-\frac{k_{12}^2}{1-\frac{\omega_1^2}{\omega^2}n_{f21}^2}\right)\widehat{I_1} + \left(k_{13}-\frac{k_{23}k_{12}}{1-\frac{\omega_1^2}{\omega^2}n_{21}^2}\right) \times \sqrt{\frac{L_3}{L_1}}\widehat{I_3} + \left(k_{14}-\frac{k_{24}k_{12}}{1-\frac{\omega_1^2}{\omega^2}n_{21}^2}\right)\sqrt{\frac{L_4}{L_1}}\widehat{I_4}$$

$$0 = \left(k_{13}-\frac{k_{23}k_{12}}{1-\frac{\omega_1^2}{\omega^2}n_{21}^2}\right)\sqrt{\frac{L_1}{L_3}}\widehat{I_1} + \left(1-\frac{\omega_1^2}{\omega^2}n_{21}^2-\frac{k_{23}^2}{1-\frac{\omega_1^2}{\omega^2}n_{21}^2}\right) \times \widehat{I_3} + \left(k_{34}-\frac{k_{23}k_{24}}{1-\frac{\omega_1^2}{\omega^2}n_{21}^2}\right)\sqrt{\frac{L_4}{L_3}}\widehat{I_4}$$

$$0 = \left(k_{14}-\frac{k_{24}k_{12}}{1-\frac{\omega_1^2}{\omega^2}n_{21}^2}\right)\sqrt{\frac{L_1}{L_4}}\widehat{I_1} + \left(k_{13}-\frac{k_{23}k_{24}}{1-\frac{\omega_1^2}{\omega^2}n_{21}^2}\right) \times \sqrt{\frac{L_3}{L_4}}\widehat{I_3} + \left(1-\frac{\omega_1^2}{\omega^2}-\frac{k_{24}^2}{1-\frac{\omega_1^2}{\omega^2}n_{f21}^2}\right)\widehat{I_4}. \quad \text{(A3)}$$

With the middle of equation (A3), the current $\widehat{I_3}$ can be expressed as

$$\widehat{I_3} = -\frac{\left(k_{13}-\frac{k_{23}k_{12}}{1-\frac{\omega_1^2}{\omega^2}n_{21}^2}\right)\sqrt{\frac{L_1}{L_3}}\widehat{I_1} + \left(k_{34}-\frac{k_{23}k_{24}}{1-\frac{\omega_1^2}{\omega^2}n_{21}^2}\right)\sqrt{\frac{L_4}{L_3}}\widehat{I_4}}{1-\frac{\omega_1^2}{\omega^2}n_{21}^2-\frac{k_{23}^2}{1-\frac{\omega_1^2}{\omega^2}n_{21}^2}}. \quad \text{(A4)}$$

By substituting (A4) into (A3), (A3) can be rewritten as

$$\hat{U}_1 = \hat{I}_1 Z_{\mathrm{pri}} - \hat{I}_4 Z_{\mathrm{mag}}$$

$$0 = \hat{I}_1 Z_{\mathrm{mag}} - \hat{I}_4 Z_{\mathrm{se}} \quad \text{(A5)}$$

where $Z_{\mathrm{pri}}\,(=Z_{\mathrm{se}})$ and Z_{mag} can be expressed, respectively, as

$$Z_{\mathrm{pri}} = Z_{\mathrm{se}} = j\omega L_1 \left\{1-\frac{\omega_1^2}{\omega^2}-\frac{\left(\kappa_{12}^2+\kappa_{13}^2\right)\left(1-\frac{\omega_1^2}{\omega^2}n_{f21}^2\right)-2\kappa_{12}\kappa_{13}\kappa_{23}}{\left(1-\frac{\omega_1^2}{\omega^2}n_{f21}^2\right)^2-\kappa_{23}^2}\right\} \quad \text{(A6)}$$

$$Z_{\mathrm{mag}} = j\omega\sqrt{L_1 L_4} \left\{\kappa_{14}-\frac{2\kappa_{12}\kappa_{13}\left(1-\frac{\omega_1^2}{\omega^2}n_{f21}^2\right)-\kappa_{23}\left(\kappa_{12}^2+\kappa_{13}^2\right)}{\left(1-\frac{\omega_1^2}{\omega^2}n_{f21}^2\right)^2-\kappa_{23}^2}\right\}. \quad \text{(A7)}$$

B. Derivation Procedure for the Phase of the Input Impedance Z_{in} in the CV Mode

The phase of the input impedance can be derived from

$$Z_{\mathrm{in}} = \frac{Z_{\mathrm{pri}}R_{L,\mathrm{eq}}}{Z_{\mathrm{se}}+R_{L,\mathrm{eq}}}. \quad \text{(A8)}$$

By multiplying both the numerator and denominator by $(-Z_{\mathrm{se}}+R_{L,\mathrm{eq}})$, the input impedance can be rewritten as

$$Z_{\mathrm{in}} = \frac{Z_{\mathrm{pri}}R_{L,\mathrm{eq}}(-Z_{\mathrm{se}}+R_{L,\mathrm{eq}})}{(Z_{\mathrm{se}}+R_{L,\mathrm{eq}})(-Z_{\mathrm{se}}+R_{L,\mathrm{eq}})}. \quad \text{(A9)}$$

As already shown in (A6) and (A7), Z_{se} is equal to Z_{pri} and only has an imaginary part. Hence, the input impedance can be expressed as

$$Z_{\mathrm{in}} = \frac{Z_{\mathrm{pri}}R_{L,\mathrm{eq}}(-Z_{\mathrm{se}}+R_{L,\mathrm{eq}})}{|Z_{\mathrm{se}}|^2+R_{L,\mathrm{eq}}^2}. \quad \text{(A10)}$$

From (A10), the real part of the input impedance can be represented as

$$\mathrm{Re}\{Z_{\mathrm{in}}\mathrm{Zin}\} = \frac{-Z_{\mathrm{pri}}R_{L,\mathrm{eq}}Z_{\mathrm{se}}}{|Z_{\mathrm{se}}|^2+R_{L,\mathrm{eq}}^2}. \quad \text{(A11)}$$

The imaginary part of the input impedance can be represented as

$$\mathrm{Im}\{Z_{\mathrm{in}}\mathrm{Zin}\} = \frac{Z_{\mathrm{pri}}R_{L,\mathrm{eq}}^2}{|Z_{\mathrm{se}}|^2+R_{L,\mathrm{eq}}^2}. \quad \text{(A12)}$$

Therefore, the phase of the input impedance can be obtained as

$$\arg\left\{\frac{\mathrm{Im}\{Z_{\mathrm{in}}\mathrm{Zin}\}}{\mathrm{Re}\{Z_{\mathrm{in}}\}}\right\} = \arg\left\{\frac{-R_{L,\mathrm{eq}}}{Z_{\mathrm{pri}}}\right\}. \quad \text{(A13)}$$

Since $Z_{\mathrm{pri}} = Z_{\mathrm{mag}}$ in the CV mode, by substituting this relationship into (A13), the phase of the input impedance can be derived as

$$\arg\left\{\frac{\mathrm{Im}\{Z_{\mathrm{in}}\mathrm{Zin}\}}{\mathrm{Re}\{Z_{\mathrm{in}}\}}\right\} = \arg\left\{\frac{-R_{L,\mathrm{eq}}}{Z_{\mathrm{mag}}}\right\}. \quad \text{(A14)}$$

REFERENCES

[1] R. Haldi and K. Schenk, "A 3.5 kW wireless charger for electric vehicles with ultra-high efficiency," in *Proc. IEEE Energy Convers. Congr. Expo.*, Sep. 2014, pp. 668–674.

[2] S. Li and C. C. Mi, "Wireless power transfer for electric vehicle applications," *IEEE J. Emerg. Sel. Topics Power Electron.*, vol. 3, no. 1, pp. 4–17, Mar. 2015.

[3] M. H. Ameri, A. Y. Varjani and M. Mohamdian, "A New Maximum Inductive Power Transmission Capacity Tracking Method," in *J. Power Electron.*, vol. 16, no. 6, pp. 2022–2011, Nov. 2016.

[4] T. D. Nguyen, S. Li, W. Li, and C. C. Mi, "Feasibility study on bipolar pads for efficient wireless power chargers," in *Proc. IEEE Appl. Power Electron. Conf. Expo.*, Mar. 2014, pp. 1676–1682.

[5] R. Bosshard, J. W. Kolar, J. Mühlethaler, I. Stevanović, B. Wunsch, and F. Canales, "Modeling and η-α-pareto optimization of inductive power transfer coils for electric vehicles," *IEEE J. Emerg. Sel. Topics Power Electron.*, vol. 3, no. 1, pp. 50–64, Mar. 2015.

[6] J. H. Kim *et al.*, "Development of 1-MW inductive power transfer system for a high-speed train," *IEEE Trans. Ind. Electron.*, vol. 62, no. 10, pp. 6242–6250, Oct. 2015.

[7] R. A. Deshmukh and D. B. Talange, "Design of 1kW inductive power transfer system for electric vehicle," in *Proc. Adv. Power Energy Conf.*, Jun. 2015, pp. 93–97.

[8] Y. Nagatsuka, N. Ehara, Y. Kaneko, S. Abe, and T. Yasuda, "Compact contactless power transfer system for electric vehicles," in *Proc. Power Electron. Conf.*, Jun. 2010, pp. 807–813.

[9] A. Pevere, R. Petrella, C. C. Mi, and Shijie Zhou, "Design of a high efficiency 22 kW wireless power transfer system for EVs fast contactless charging stations," in *Proc. IEEE Electr. Veh. Conf.*, Dec. 2014, pp. 1–7.

[10] G. Covic and J. Boys, "Modern trends in inductive power transfer for transportation applications," *IEEE J. Emerg. Sel. Topics Power Electron.*, vol. 1, no. 1, pp. 28–41, Mar. 2013.

[11] J. Deng, J. Deng, W. Li, S. Li, and C. Mi, "Magnetic integration of LCC compensated resonant converter for inductive power transfer applications," in *Proc. IEEE Energy Convers. Congr. Expo.*, Sep. 2014, pp. 660–667.

[12] T. Shijo, K. Ogawa, and S. Obayashi, "Optimization of thickness and shape of core block in resonator for 7 kW-class wireless power transfer system for PHEV/EV charging," in *Proc. IEEE Energy Convers. Congr. Expo.*, Sep. 2015, pp. 3099–3102.

[13] W. Zhang, J. C. White, A. M. Abraham, and C. C. Mi, "Loosely coupled transformer structure and interoperability Study for EV wireless charging systems," *IEEE Trans. Power Electron.*, vol. 30, no. 11, pp. 6356–6367, Nov. 2015.

[14] A. Kurs, A. Karalis, R. Moffatt, J. D. Joannopoulos, P. Fisher, and M. Soljacic, "Wireless power transfer via strongly coupled magnetic resonances," *Science*, vol. 317, no. 5834, pp. 83–86, Jul. 2007.

[15] T. C. Beh, M. Kato, T. Imura, S. Oh, and Y. Hori, "Automated impedance matching system for robust wireless power transfer via magnetic resonance coupling," *IEEE Trans. Ind. Electron.*, vol. 60, no. 9, pp. 3689–3698, Sep. 2013.

[16] D. Ahn and S. Hong, "A study on magnetic field repeater in wireless power transfer," *IEEE Trans. Ind. Electron.*, vol. 60, no. 1, pp. 360–371, Jan. 2013.

[17] S. Moon, B. C. Kim, S. Y. Cho, C. H. Ahn, and G. W. Moon, "Analysis and design of a wireless power transfer system with an intermediate coil for high efficiency," *IEEE Trans. Ind. Electron.*, vol. 61, no. 11, pp. 5861–5870, Nov. 2014.

[18] W. X. Zhong, C. Zhang, X. Liu and S. Y. R. Hui, "A methodology for making a three-coil wireless power transfer system more energy efficient than a two-coil counterpart for extended transfer distance," *IEEE Trans. Power Electron.*, vol. 30, no. 2, pp. 933–942, Feb. 2015.

[19] S. Moon and G. W. Moon, "Wireless power transfer system with an asymmetric four-coil resonator for electric vehicle battery chargers," *IEEE Trans. Ind. Electron.*, vol. 31, no. 10, pp. 6844–6854, Oct. 2016.

[20] D. H. Tran, V. B. Vu, V. L. Pham, and W. Choi, "Design and implementation of high efficiency wireless power transfer system for on-board charger of electric vehicle," in *Proc. IEEE Power Electron. Motion Control Conf.*, May 2016, pp. 2466–2469.

[21] Q. Zhu, L. Wang, and C. Liao, "Compensate capacitor optimization for kilowatt-level magnetically resonant wireless charging system," *IEEE Trans. Ind. Electron.*, vol. 61, no. 12, pp. 6758–6768, Dec. 2014.

[22] C. Zheng *et al.*, "High efficiency contactless power transfer system for electric vehicle battery charging application," *IEEE J. Emerg. Sel. Topics Power Electron.*, vol. 3, no. 1, pp. 65–74, Mar. 2015.

[23] R. Bosshard, J. W. Kolar, and B. Wunsch, "Control method for Inductive Power Transfer with high partial-load efficiency and resonance tracking," in *Proc. IEEE Power Electron. Conf.*, May 2014, pp. 2167–2174.

[24] J. A. Sabate, M. M. Jovanovic, F. C. Lee, and R. T. Gean, "Analysis and design-optimization of LCC resonant inverter for high-frequency AC distributed power system," *IEEE Trans. Ind. Electron.*, vol. 42, no. 1, pp. 63–71, Feb. 1995.

Duc Hung Tran was born in Bac Giang, Vietnam, in 1988. He received the B.S. degree from the Hanoi University of Science and Technology, Hanoi, Vietnam, in 2014, and the M.S. degree from Soongsil University, Seoul, South Korea, in 2017, both in electrical engineering.

His research interests include wireless power transfer, dc–dc converters dealing with the renewable sources and batteries for energy storage system or hybrid electric vehicles, and soft-switching techniques for the pulse width modulation/pulse-frequency modulation converters.

Van Binh Vu received the B.S. degree from the Hanoi University of Science and Technology, Hanoi, Vietnam, in 2014, and the M.S. degree from Soongsil University, Seoul, South Korea, in 2016, both in electrical engineering. He is currently working toward the Ph.D. degree in the School of Electrical and Electronic Engineering, Newcastle University, Newcastle upon Tyne, U.K.

His current research interests include wireless power transfer and resonant converter for electric vehicles.

Mr. Vu received the International Postgraduate Research Studentship by Soongsil University in 2014 and Newcastle - Singapore Studentship by Newcastle University and National University of Singapore in 2016.

Woojin Choi (S'00–M'05) was born in Seoul, South Korea, in 1967. He received the B.S. and M.S. degrees from Soongsil University, Seoul, South Korea, in 1990 and 1995, respectively, and the Ph.D. degree from Texas A &M University, College Station, TX, USA, in 2004, all in electrical engineering.

He was a Research Engineer with Daewoo Heavy Industries, Seoul, from 1995 to 1998. In 2005, he joined the School of Electrical Engineering, Soongsil University. His research interests include modeling and control of electrochemical energy sources, such as fuel cells, batteries, and supercapacitors; power conditioning technologies in renewable energy systems; and dc–dc converters for electric vehicles and fuel cells.

Dr. Choi is an Associate Editor of the IEEE TRANSACTIONS ON INDUSTRY APPLICATIONS and a Publication Editor of the *Journal of Power Electronics of the Korean Institute of Power Electronics*.